IJNAOE
©SNAK, 2014

Int. J. Nav. Archit. Ocean Eng. (2014) 6:363~379
http://dx.doi.org/10.2478/IJNAOE-2013-0185
pISSN: 2092-6782, eISSN: 2092-6790

Experimental investigation of frictional resistance reduction with air layer on the hull bottom of a ship

Jinho Jang, Soon Ho Choi, Sung-Mok Ahn, Booki Kim and Jong Soo Seo

SSMB (Samsung Ship Model Basin), Marine Research Institute, Samsung Heavy Industries Co., Ltd., Korea

ABSTRACT: *In an effort to cope with recent high oil price and global warming, developments of air lubricated ships have been pursued to reduce greenhouse gas emissions and to save fuel costs by reducing the frictional resistance. In this study, reduction in the frictional resistance by air lubrication with air layers generated on the lower surface of a flat plate was investigated experimentally in the large water tunnel of SSMB. The generated air layers were observed, and changes in the local frictional drag were measured at various flow rates of injected air. The results indicated that air lubrication with air layers might be useful in reducing the frictional resistance at specific conditions of air injection. Accordingly, resistance and self-propulsion tests for a 66K DWT bulk carrier were carried out in the towing tank of SSMB to estimate the expected net power savings.*

KEY WORDS: Greenhouse gas emissions; Fuel costs; Frictional resistance; Air lubrication; Air layer; Air injection; Net power savings.

INTRODUCTION

The frictional resistance of a ship is one of major resistance components, approximately 60~70% of the total resistance. Therefore, if significant reduction in the frictional resistance is achieved, it will be useful in reducing greenhouse gas emissions and saving fuel costs consequently.

Air lubrication techniques can reduce the skin friction using air layers or artificial air cavities generated on the wetted hull surface by air injection (Bushnell and Hefner, 1990; Ceccio, 2010a). Some of the basic ideas had been proposed in the 19th century already (Latorre, 1997). However, some technical issues should be resolved for practical applications to large vessels sailing the ocean (Ceccio et al., 2010b): Hull attitude changes during turning or ship motions in waves may hinder resistance reduction with air lubrication by making air-water flows unstable. Moreover, an expensive air supply system should be installed to inject the right amount of air on the hull bottom surface of a large ocean-going vessel and the maintenance of the system should be considered as well. Nevertheless, air lubrication techniques are getting more attention as an effective means to save fuel costs in shipping industries because a recent surge in oil prices might shorten the payback period of an air supply system (Allenström and Leer-Andersen, 2010; Foeth, 2008; Foeth et al., 2010; Hoang et al., 2009; Insel et al., 2010; Thill, 2010).

Corresponding author: *Jinho Jang*, e-mail: *jinho1.jang@samsung.com*

This paper has been selected from the Proceedings of PRADS 2013, reviewed by referees and modified to meet guidelines for publication in IJNAOE.

Recently, Mitsubishi Heavy Industries developed MALS (Mitsubishi Air Lubrication System), which has been applied to two module carriers of NYK-Hinode Line, a coal carrier built by Oshima Shipbuilding, a ferry of Japan's A-Line Ferry. It was announced that net power savings up to about 13% were obtained from the sea trials of the module carriers (Mizokami et al., 2010; Mizokami et al., 2011; Tanaka, 2011).

In this study, the feasibility of air lubrication technique without any significant changes of the hull form was investigated experimentally. Firstly, the experiments to generate air layers on the lower surface of a flat plate in the large water tunnel of SSMB were conducted The generated air layers were observed, and changes in the local frictional drag were measured. Secondly, resistance and self-propulsion tests for a 66K Supramax bulk carrier were carried out in the towing tank of SSMB. Air layers generated on the hull bottom were observed, and changes in the resistance and propulsion performance were investigated, and the expected net power savings were estimated.

FRICTIONAL DRAG REDUCTION WITH AIR LAYER

When air is injected into the boundary layer of the wetted surface, an air-water mixture flow containing both air bubbles and water can be formed. If the amount of injected air increases, air bubbles begin to coalesce into patches that cover the surface continuously, and a transitional air layer where the patches coexist with air bubbles is formed as shown in Fig. 1(Left). The frictional drag on the surface covered with a continuous air layer can be reduced effectively as if the wetted surface area were reduced because the friction with water may change into that with air (Bushnell and Hefner, 1990). Therefore, on the surface covered with a transitional air layer, it is expected that both air bubbles and patches of continuous air contribute to the frictional drag reduction. Elbing et al. (2008) described that reduction in the local frictional drag can be achieved from about 20% to 80% on the surface covered with a transitional air layer. If the amount of injected air is increased more, coalescence of air bubbles is promoted further and a fully continuous air layer covering the wetted surface on a large scale is developed as shown in Fig. 1(Right) and reduction in the local frictional drag can reach more than 80% (Elbing et al., 2008; Ceccio, 2010a).

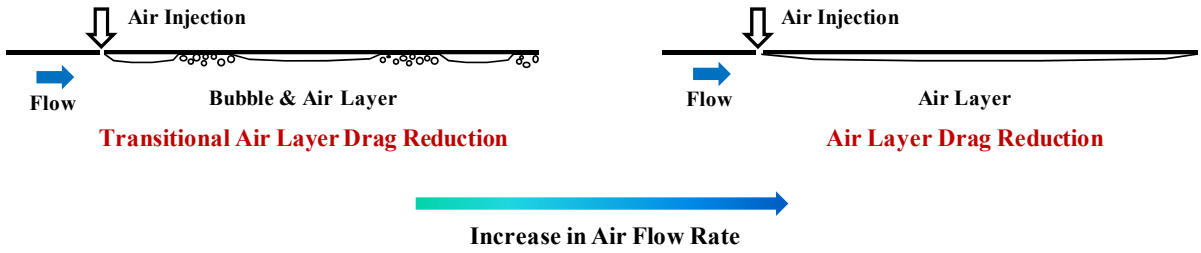

Fig. 1 Schematic figure of drag reduction with air layer, reproduced from Ceccio and Makihärju (2012).

GENERATION OF AIR LAYER UNDER A FLAT PLATE

Experiments with a flat plate were conducted in the large water tunnel. The experimental configuration is shown in the schematic drawing of Fig. 2. Air layers were generated on the lower surface of the flat plate horizontally mounted in the water tunnel to investigate the feasibility of air lubrication for reducing the frictional resistance of ships by injecting air on the bottom of the hull.

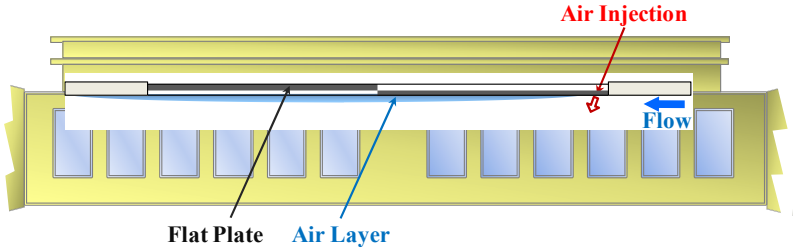

Fig. 2 Experimental configuration for generation of air layer under a flat plate in the water tunnel.

Experimental setup

A flat plate with length of 7.5*m*, width of 1.0*m* and thickness of 8*cm* was mounted horizontally in the test section of the water tunnel as shown in Fig. 3. Air was injected through a flush mounted slit with gap of 1.5*mm* and width of 0.77*m* near the front end of the flat plate.

In order to measure the changes in the local frictional drag by air layers, two floating-plate-type friction sensors were installed flushing with the lower surface of the flat plate. The centers of the sensors were located at 1.1*m* and 4.3*m* from the leading edge of the flat plate.

Air was injected according to the diagram shown in Fig. 4. The pressure of compressed air was controlled by a pressure regulator to adjust flow rates of injected air, and the flow rates were measured by a flow meter.

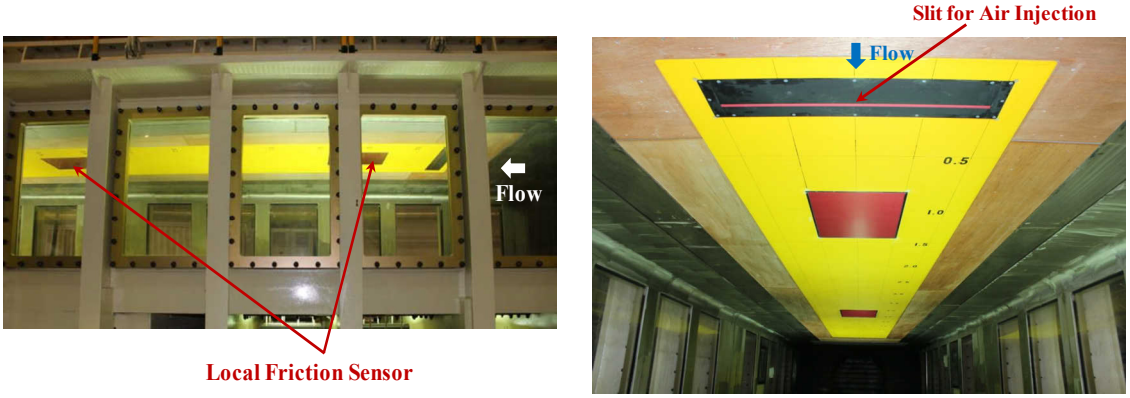

Fig. 3 Flat plate in the water tunnel for generation of air layer.

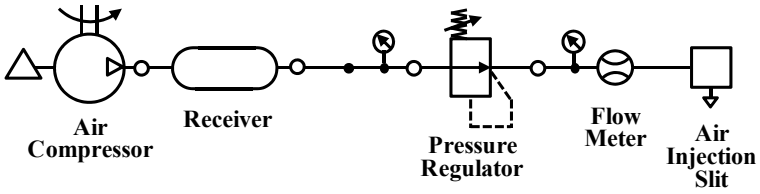

Fig. 4 Air supply chain for air injection.

Results of the experiment

Air layers generated on the lower surface of the flat plate at various flow rates of injected air were observed, and changes in the local frictional drag were measured. Captured images of typical air layers and measured results of changes in the local frictional drag when the inflow speed was 5*m/s* were shown in Figs. 5~10. Especially, Figs. 8~10 contain the results obtained when the flat plate had side walls, 10*mm* high, to suppress air leakage at both sides. The ideal air layer thickness, t_{AL} in Eq. (1) was used as a parameter to describe the flow rate of injected air although it is an ideal or imaginary value. In Figs. 7 and 10, 0% frictional drag reduction means that the frictional drag is not reduced at all, and 100% means that the frictional drag is perfectly disappeared.

$$t_{AL} = \frac{Q_{Air}}{V_{Inflow} \cdot B_{Air}} \tag{1}$$

In Eq. (1), Q_{Air}, V_{Inflow}, and B_{Air} are volume flow rate of injected air, inflow speed, and the width of the air injection slit, respectively. Flow rates of air at normal condition, 1*atm* and 0°*C* measured by a flow meter were converted into corresponding flow rates of air at the pressure and temperature in the test section measured at each run.

Firstly, we examined the case where the flat plate had no side wall in Figs. 5~7. As the flow rate of injected air increased, reduction in the frictional drag was enhanced on the floating plate of the fore local friction sensor: about 20% reduction in the local frictional drag at $t_{AL} \cong 2mm$ and more than 80% reduction when $t_{AL} > 5.5mm$ were obtained as shown in Fig. 5.

Although it is difficult to distinguish clearly from the captured images of air layers in Figs. 6 and 7, it is thought that a transitional air layer when roughly $2mm < t_{AL} < 5.5mm$ and a continuous air layer when $t_{AL} > 5.5mm$ were generated on the fore part of the flat plate if a classification by Elbing et al. (2008) according to levels of reduction in the friction drag is accepted.

On the floating plate of the aft local friction sensor, reduction in the frictional drag showed a similar tendency as the flow rate of injected air increased up to $t_{AL} \cong 6mm$: about 50% reduction in the frictional drag was obtained at $t_{AL} \cong 6mm$. However, as the flow rate of air increased over $t_{AL} = 6mm$, the amount of reduction in the frictional drag declined and reduction in the frictional drag was only about 15% even at $t_{AL} \cong 10mm$. At $t_{AL} = 3.5mm$, the air layer generated on the aft part of the flat plate shown in Fig. 7 looks similar to that generated on the fore part shown in Fig. 6. Whereas at $t_{AL} = 10.1mm$, it is observed that the air layer was split into left and right in front of the aft local friction sensor, and then the bulk of air flowed downstream along both sides of the flat plate as shown in Fig. 7. It is thought that this phenomenon occurred because a lot of air flowed into streamwise vortices generated along both sides of the air injection slit due to a speed difference between injected air and water flow, and a continuous air layer was not fully developed on the floating plate of the aft local friction sensor.

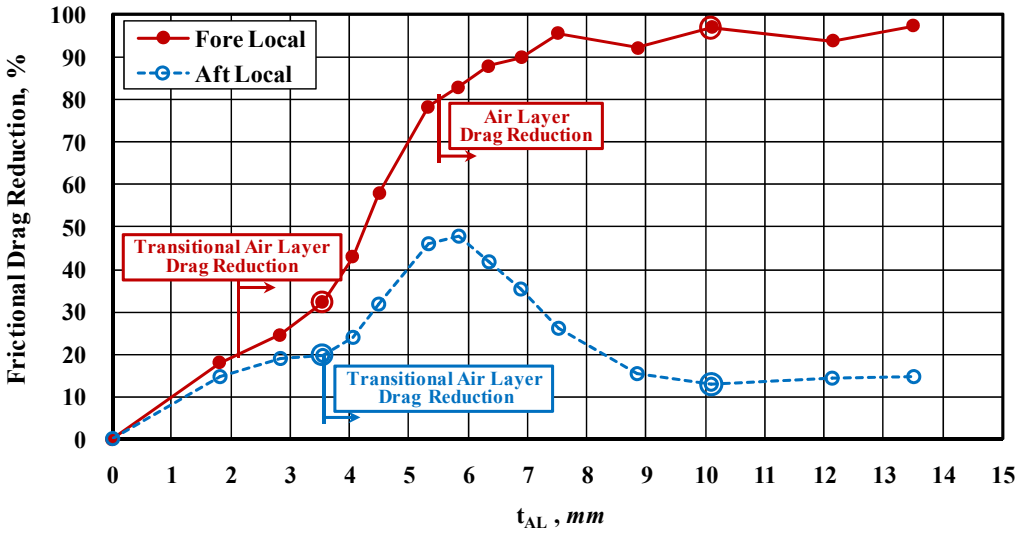

Fig. 5 Frictional drag reduction without side wall at $V_{Inflow} = 5m/s$.

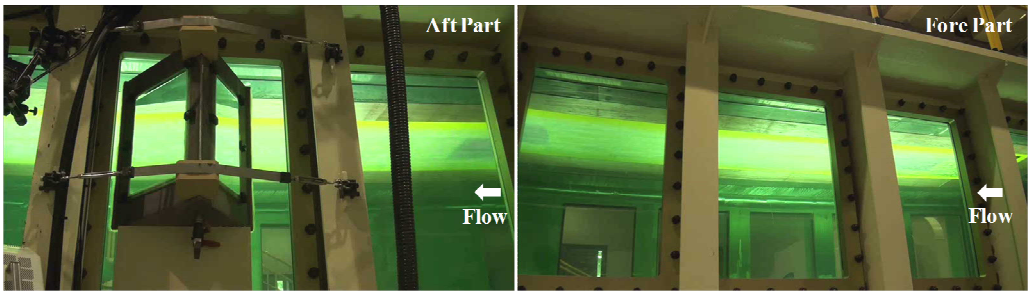

Fig. 6 Air layer under the flat plate without side wall at $V_{Inflow} = 5m/s$ and $t_{AL} = 3.5mm$.

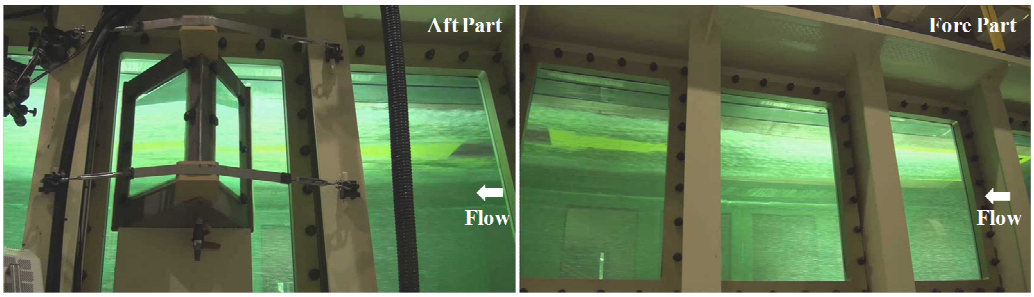

Fig. 7 Air layer under the flat plate without side wall at $V_{Inflow} = 5m/s$ and $t_{AL} = 10.1mm$.

Secondly, we examined the case where the flat plate had side walls 10*mm* high at both sides in Figs. 8~10. As the flow rate of injected air increased, reduction in the local frictional drag was enhanced on the floating plates of the aft local friction sensor as well as the fore one. Therefore, as shown in Fig. 8, about 20% and more than 80% of local frictional drag on the floating plates of both local friction sensors were reduced at $t_{AL} \cong 2.5mm$ and $t_{AL} > 8.5mm$, respectively. From the captured images in Figs. 9 and 10, splitting of the air layers was not observed unlike the case where the flat plate had no side wall. It seems that the side walls contributed to weakening the strength of the streamwise vortices and reducing air leakage into both sides of the flat plate. It is thought that a transitional air layer at $2.5mm < t_{AL} < 8.5mm$ and a continuous air layer when $t_{AL} > 8.5mm$ were generated on the whole surface of the flat plate by the classification by Elbing et al. (2008) as previously stated.

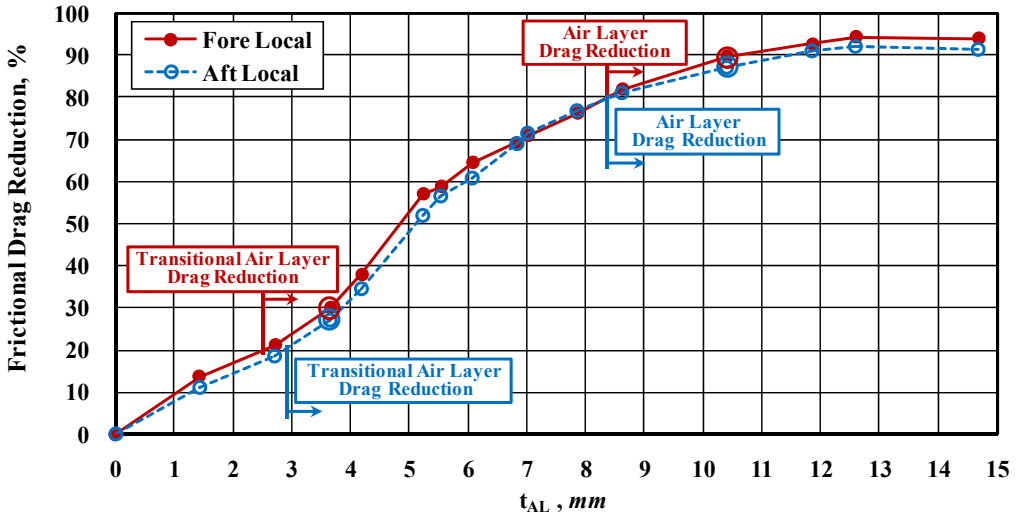

Fig. 8 Frictional drag reduction with side walls 10*mm* high at $V_{Inflow} = 5m/s$.

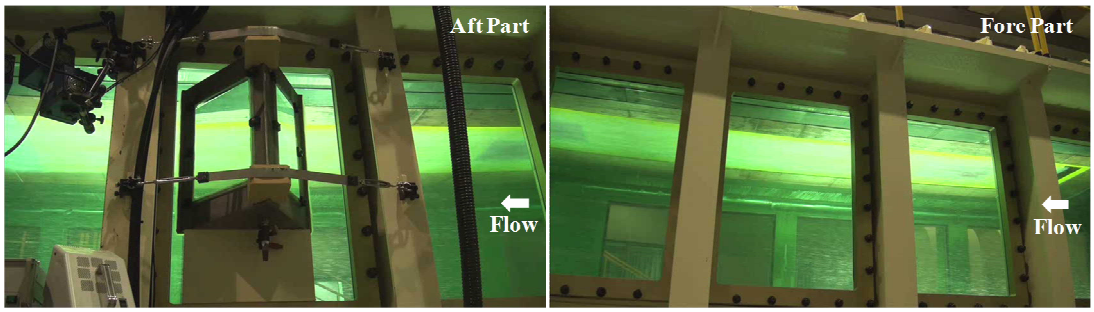

Fig. 9 Air layer under the flat plate with side walls 10*mm* high at $V_{Inflow} = 5m/s$ and $t_{AL} = 3.7mm$.

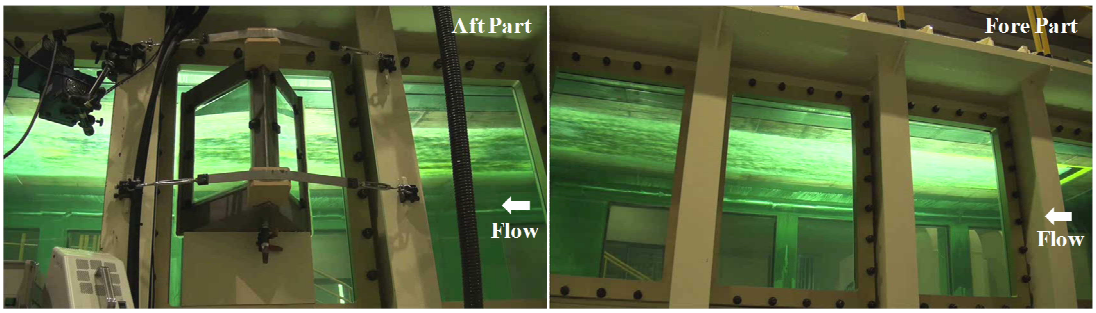

Fig. 10 Air layer under the flat plate with side walls 10*mm* high at $V_{Inflow} = 5m/s$ and $t_{AL} = 10.4mm$.

ESTIMATION OF POWER SAVINGS OF A SHIP

A series of resistance and self-propulsion tests for a wide beam bulk carrier was carried out in the towing tank to investigate net energy savings with air layers generated on the hull bottom by air injection.

66K DWT Supramax bulk carrier

A 66K DWT Supramax bulk carrier was selected as a test hull form and a model ship was manufactured with a scale ratio of 24.0 to perform the resistance and self-propulsion tests.

The principal particulars of the ship and a stock propeller are shown in Tables 1 and 2, and a body plan of the ship is shown in Fig. 11. The flat bottom area, where reduction in the frictional resistance can be expected to occur, is about 42.5% of the total wetted surface area.

Table 1 Principal particulars of 66K DWT supramax bulk carrier.

Principal particulars	
Length overall, L_{OA}	200.0*m*
Length between perpendiculars, L_{BP}	192.0*m*
Breadth, B	36.0*m*
Draft, T	11.2*m*
Length on waterline, L_{WL}	196.0*m*
Displacement volume, ∇	65012.3m^3
Wetted surface area, S	9909.6m^2
Block coefficient, C_B	0.8399
Model scale ratio, λ	24.0

Table 2 Principal particulars of stock propeller.

Principal Particulars	
Diameter, D	6.0*m*
Number of blades, Z	4
$(P/D)_{Mean}$	0.709
Expanded area ratio	0.473
Section	NACA66

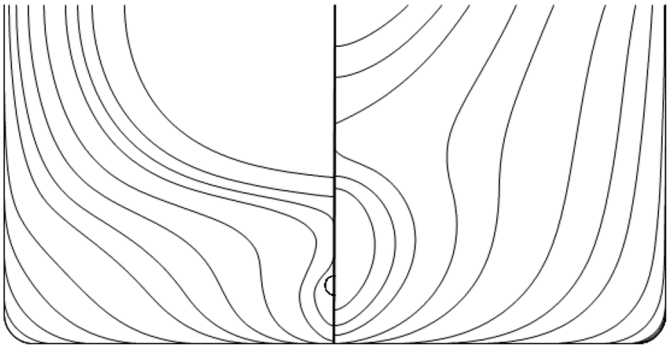

Fig. 11 Body plan of 66K DWT supramax bulk carrier.

Test setup

Six air injection units that operate independently were installed to the model ship as shown in Fig. 12. Three units, [U1-P], [U1-C], and [U1-S] were located at the 17th station and the other three units, [U2-P], [U2-C], and [U2-S] were located at the 15th station. In order to avoid undesirable increase in the resistance, the air injection units were mounted flushing with the bottom surface of the hull.

Air was injected through array of holes on the base plate of each air injection unit according to the air supply chain as shown in Fig. 13. Compressed air by an air compressor was stored in the air receivers on the deck of the model ship and the flow rate of air supplied to the air injection units were adjusted by PC-controlled mass flow meters.

The model ship prepared for the tests in the towing tank is shown in Fig. 14. In order to avoid any interference, the tube to supply air from the air compressor to the air receivers in the model ship was disconnected during each test run.

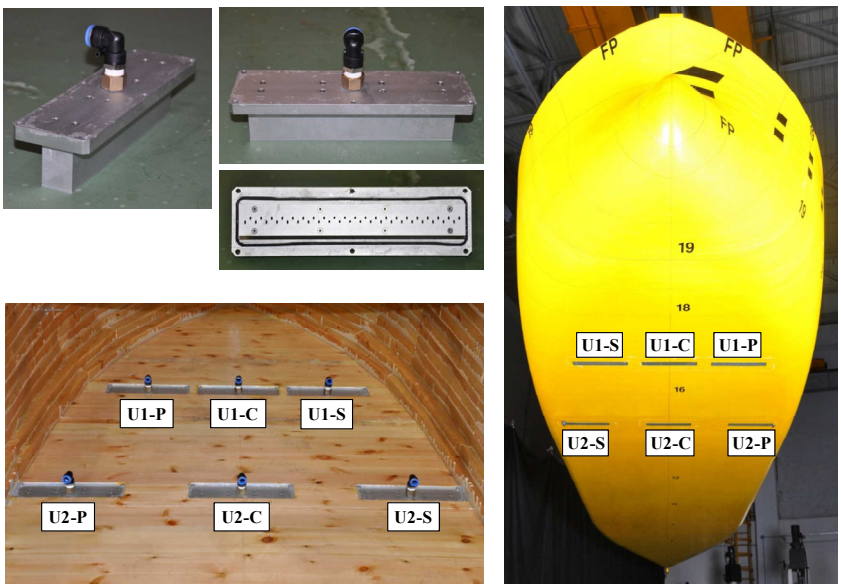

Fig. 12 Arrangement of air injection units.

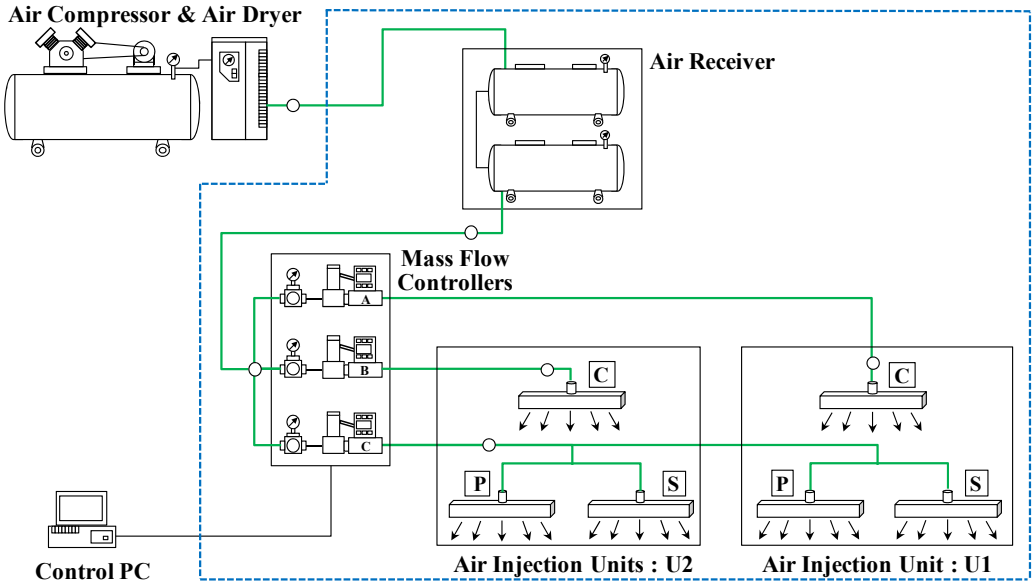

Fig. 13 Air supply chain for air injection in the towing tank.

Fig. 14 Model ship prepared for the resistance test in the towing tank.

Procedures to estimate changes in the power by air layer

Effective power

The effective power when air is not injected, P_E was estimated using a well-known procedure in Eqs. (2) and (3).

$$C_{TS} = \left(\frac{S + S_{BK}}{S}\right)(C_{FS} + C_A) + C_R + C_{AA} \tag{2}$$

$$P_E = R_{TS} \cdot V_S \tag{3}$$

In Eqs. (2) and (3), C_T is the total resistance coefficient, C_F is the frictional resistance coefficient, C_A is the model-ship correlation allowance coefficient, C_R is the residuary resistance coefficient, C_{AA} is the air resistance coefficient, S is the wetted surface area of the hull, S_{BK} is the wetted surface area of the bilge keels, R_T is the total resistance, and V is the ship speed. The subscript "S" denotes full scale value. The frictional resistance coefficient when air is not injected is obtained from the ITTC 1957 model-ship correlation line.

The effective power when air is injected, $P_{E,Air}$ was estimated according to Eqs. (7) and (8) on the assumptions that air injection does not influence the residuary resistance and reduction ratio of the frictional resistance in the full scale is kept the same level as the model scale in Eqs. (4)~(6).

$$C_{R,Air} = C_R \tag{4}$$

$$C_{FM,Air} = C_{TM,Air} - C_R \tag{5}$$

$$\frac{C_{FM,Air}}{C_{FM}} = \frac{C_{FS,Air}}{C_{FS}} \tag{6}$$

$$C_{TS,Air} = \left(\frac{S + S_{BK}}{S}\right)(C_{FS,Air} + C_A) + C_{R,Air} + C_{AA} \tag{7}$$

$$P_{E,Air} = R_{TS,Air} \cdot V_S \tag{8}$$

In Eqs. (4)~(8), the subscript "Air" denotes the case where air is injected and the subscript "M" is model scale value.

$$\Delta R_{TM} = \left(1 - \frac{R_{TM,Air}}{R_{TM}}\right) \times 100 \tag{9}$$

$$\Delta P_E = \left(1 - \frac{P_{E,Air}}{P_E}\right) \times 100 \tag{10}$$

Finally, reductions in the total resistance of the model ship and the effective power are obtained according to Eqs. (9) and (10).

Delivered power

When air is not injected, the towing force to be supplied to the model ship for skin friction correction was determined by Eq. (11). The full scale wake fraction was corrected from the model scale wake fraction and the thrust deduction fraction obtained from the self-propulsion tests according to Eq. (12) based on Tanaka-Sasajima method. The advance ratio of the full scale propeller was obtained from the full scale propeller loading coefficient in Eq. (13).

$$F_D = \frac{1}{2}\rho_M S_M V_M{}^2 \cdot \{C_{FM} - (C_{FS} + C_A)\} \tag{11}$$

$$w_{TS} = (t + 0.04) + (w_{TM} - t - 0.04)\frac{C_{FS} + C_A}{C_{FM}} \tag{12}$$

$$\left(\frac{K_T}{J^2}\right) = \frac{S}{2D^2}\frac{C_{TS}}{(1-t)(1-w_{TS})^2} \tag{13}$$

F_D is the towing force, w_T is the effective wake fraction, t is the thrust deduction fraction, (K_T/J^2) is the loading coefficient of the full scale propeller, and D is the propeller diameter.

Likewise, when air is injected, the towing force ($F_{D,Air}$), the effective wake fraction ($w_{TS,Air}$), and the propeller loading coefficient $(K_T/J^2)_{Air}$ were obtained according to Eqs. (14)~(16).

$$F_{D,Air} = \frac{1}{2}\rho_M S_M V_M{}^2 \cdot \{C_{FM,Air} - (C_{FS,Air} + C_A)\} \tag{14}$$

$$w_{TS,Air} = (t_{Air} + 0.04) + (w_{TM,Air} - t_{Air} - 0.04)\frac{C_{FS,Air} + C_A}{C_{FM,Air}} \tag{15}$$

$$\left(\frac{K_T}{J^2}\right)_{Air} = \frac{S}{2D^2}\frac{C_{TS,Air}}{(1-t_{Air})(1-w_{TS,Air})^2} \tag{16}$$

The quasi-propulsive efficiency, η_D was estimated from the physical quantities at the self-propulsion point obtained using Eqs. (11)~(16).

Finally, delivered power savings were obtained according to Eq. (17).

$$\Delta P_D = \left(1 - \frac{P_{D,Air}}{P_D}\right) \times 100 \tag{17}$$

Test results

Resistance reduction

Resistance tests of the 66K Supramax bulk carrier were performed at design draft to investigate the resistance reduction with air layers in various test conditions such as combinations of air injection units and flow rates of injected air. In this paper, noteworthy results among whole test results are discussed.

Firstly, air was injected from all injection units at the towing speed corresponding to 14.5*knots*, the design speed of the ship. The flow rates of air were set to 100 and 250 *SLPM* from the center injection units of [U1-C] and [U2-C], respectively. Sum of the air flow rates from the side injection units, [U1-P], [U1-S], [U1-P], and [U1-S] were changed to be 100, 200, and 300 *SLPM*. Here, *SLPM* denotes liter per minute at standard condition, 1*atm* and 25°*C* as shown in Table 3. Fig. 15 represents total resistance reduction of the model ship (ΔR_{TM}) and effective power reduction (ΔP_E) compared to the values when air was not injected.

Table 3 Air injection condition I (air injection from all units) at V_S = 14.5*knots*.

Condition	$Q_{Std.Air}$ at Air Injection Unit in Model Scale [*SLPM*]				Mean t_{AL} [*mm*]
	[U1-C]	[U1-P & S] [U2-P & S]	[U2-C]	Total	
I-A	100	100	250	450	4.1
I-B	100	200	250	550	4.6
I-C	100	300	250	650	5.1

When air was injected with the flow rates of 100 *SLPM* from a center injection unit [U1-C], 250 *SLPM* from the other center injection unit [U2-C], and 200 *SLPM* from the side injection units [U1-P], [U1-S], [U2-P], and [U2-S], the resistance of the model ship was reduced by about 9%, and an effective power reduction was estimated to be about 7%. It is thought that a transitional air layer was well developed over the wide area of the bottom as shown in the captured image of Fig. 16. However, it was observed that a significant amount of air was leaking toward the hull side around the 12th station, and it seemed that this air leakage might cause an additional increase in the resistance by disturbing the flow around the hull.

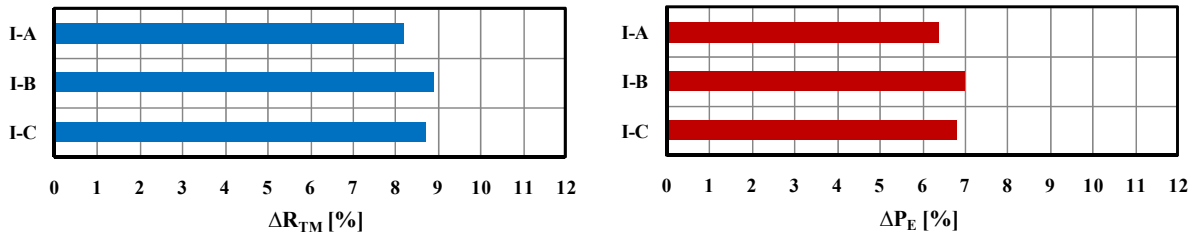

Fig. 15 Reduction in the resistance and effective power at V_S = 14.5*knots* in the air injection condition I.

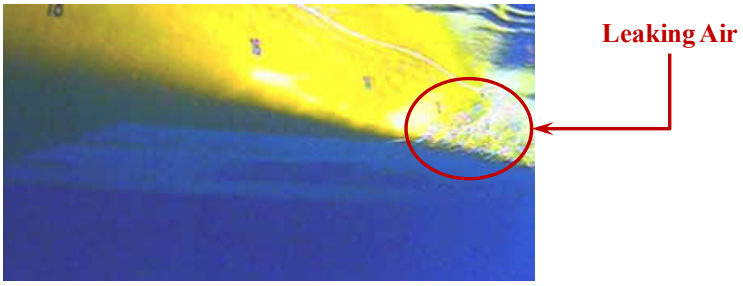

Fig. 16 Captured air layer at V_S = 14.5*knots* in the air injection condition I-B.

Secondly, air was injected from the only center injection units at the same towing speed as the previous case. With the unchanged flow rate of 100 *SLPM* from the unit [U1-C], the flow rate of air from the unit [U2-C] was changed to 200, 250, 300, and 350 *SLPM* as shown in Table 4. It is shown that the total resistance of the model ship and effective power were reduced up to about 11% and 9%, respectively when air was injected with the flow rate of 100 *SLPM* from the unit [U1-C] and 300 *SLPM* from the unit [U2-C] in Fig. 17. These results show that more resistance reduction was obtained when air was injected from the center units of [U1-C] and [U2-C] only, compared to the case of air injection from all units including the side. In other words, the side injection units [U1-P], [U1-S], [U2-P], and [U2-S] did not make any contribution to the reduction in the resistance and effective power under the current arrangement of the air injection units.

Table 4 Air injection condition II (air injection from units [U1-C] and [U2-C]) at V_S = 14.5*knots*.

Condition	$Q_{Std.Air}$ at Air Injection Unit in Model Scale [*SLPM*]			Mean t_{AL} [*mm*]
	[U1-C]	[U2-C]	Total	
II-A	100	200	300	6.2
II-B	100	250	350	7.2
II-C	100	300	400	8.2
II-D	100	350	450	9.2

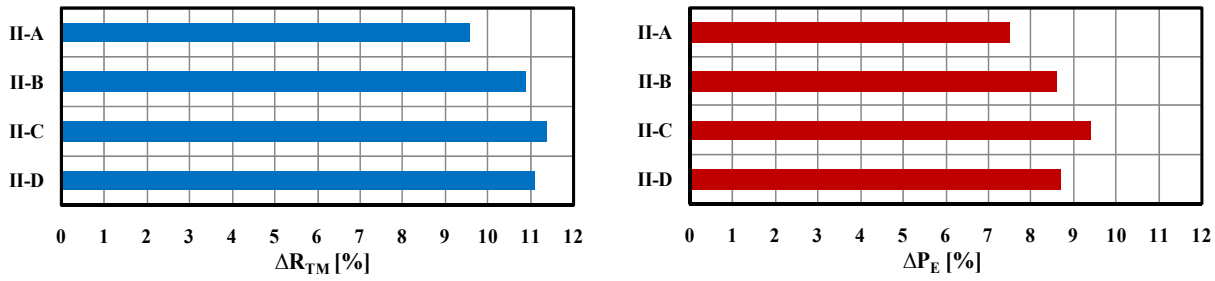

Fig. 17 Reduction in the resistance and effective power at V_S = 14.5*knots* in the air injection condition II.

Lastly, additional tests were performed at 13.0 and 16.0*knots* with air injection from the center units [U1-C] and [U2-C] according to the air injection condition II-C in Table 4. Air was injected with the flow rates corresponding to mean t_{AL} = 8.2*mm* at each test speed. Fig. 18 presents the air injection effects with variation in speed. The resistance and effective power were reduced by 10 to 12% and 8 to 10%, respectively. It seems that the air layers on the bottom of the hull are similar in shape from the images captured during the resistance tests in Fig. 19.

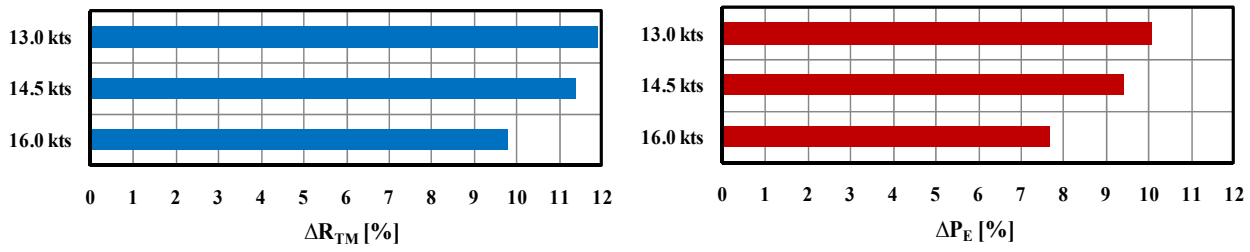

Fig. 18 Reduction in the resistance and effective power at mean t_{AL} = 8.2*mm* in the air injection condition II.

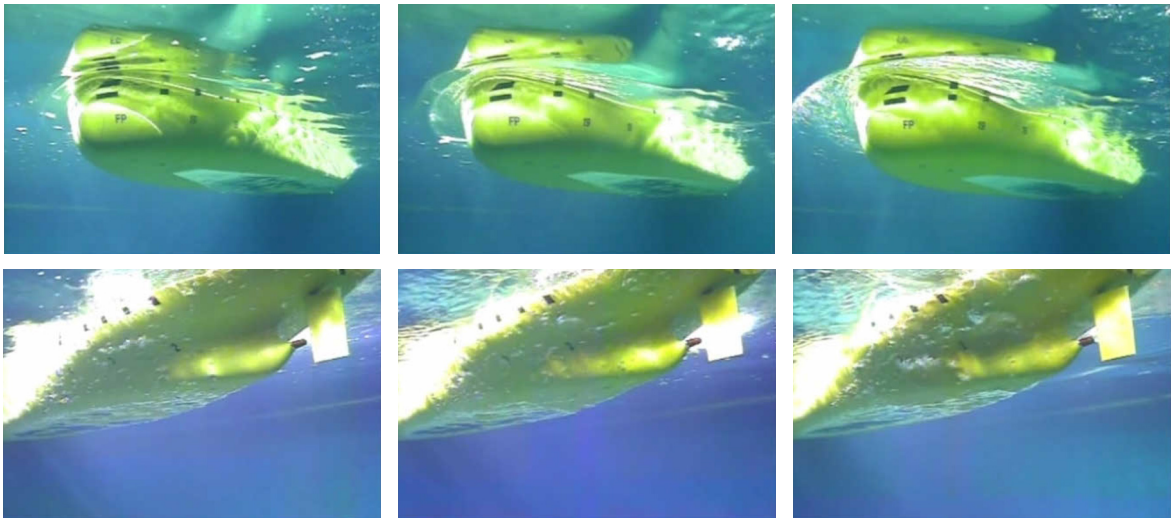

(a) V_S = 13.0*knots*. (b) V_S = 14.5*knots*. (c) V_S = 16.0*knots*.

Fig. 19 Air layers captured during resistance tests at mean t_{AL} = 8.2*mm* in the air injection condition II.

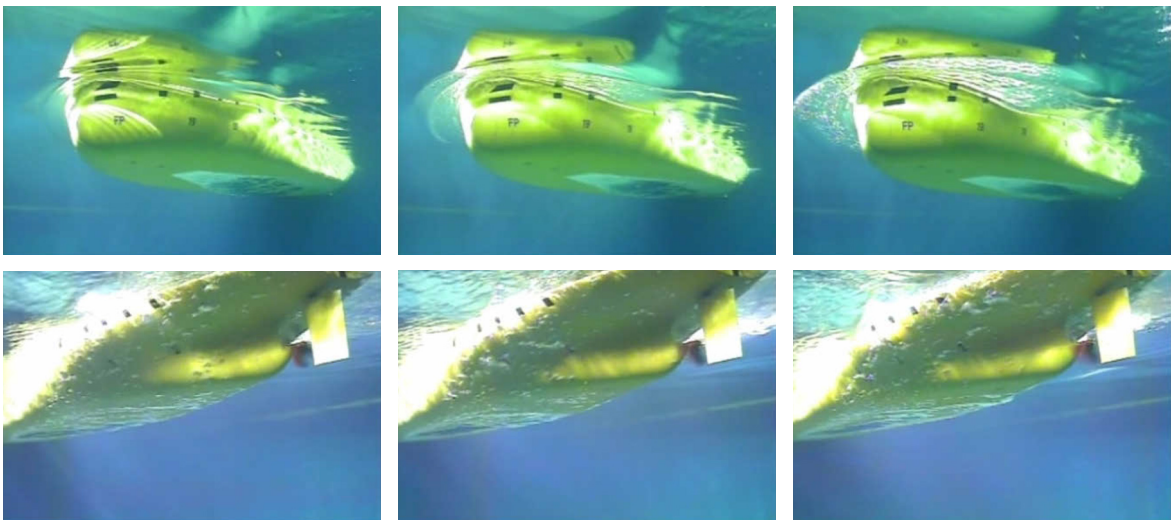

(a) V_S = 13.0*knots*. (b) V_S = 14.5*knots*. (c) V_S = 16.0*knots*.

Fig. 20 Air layers captured during self-propulsion tests at mean t_{AL} = 8.2*mm* in the air injection condition II.

Effects of air layer on the propulsion performance

Self-propulsion tests of the 66K Supramax bulk carrier were performed at design draft, 11.2*m* to investigate effects of air layers on the propulsion performance when air was injected with the flow rates corresponding to mean t_{AL} = 8.2*mm*, the same ideal air layer thickness as the air injection condition mentioned at the end of the previous section, from the units [U1-C] and [U2-C] according to the air injection condition II-C in Table 4..

The captured images of the air layers from the resistance and self-propulsion tests are show in Figs. 19 and 20 and it is shown that the air layers similar in shape were generated on the bottom of the hull. It seems that the propeller suction almost did not affect the amount of air bubbles flowing into the propeller plane.

Fig. 21 shows the changes in the towing force (F_D), propeller thrust (T_M) and propeller torque (Q_M) measured during the self-propulsion tests when the rate of revolution of the propeller was 9.0*rps* near the self-propulsion point at 14.5*knots*. Air was injected in 20*seconds* after the measurement started. When a stable air layer was generated on the bottom of the hull by air injection, the propeller thrust and torque was reduced significantly, while the towing force level was maintained.

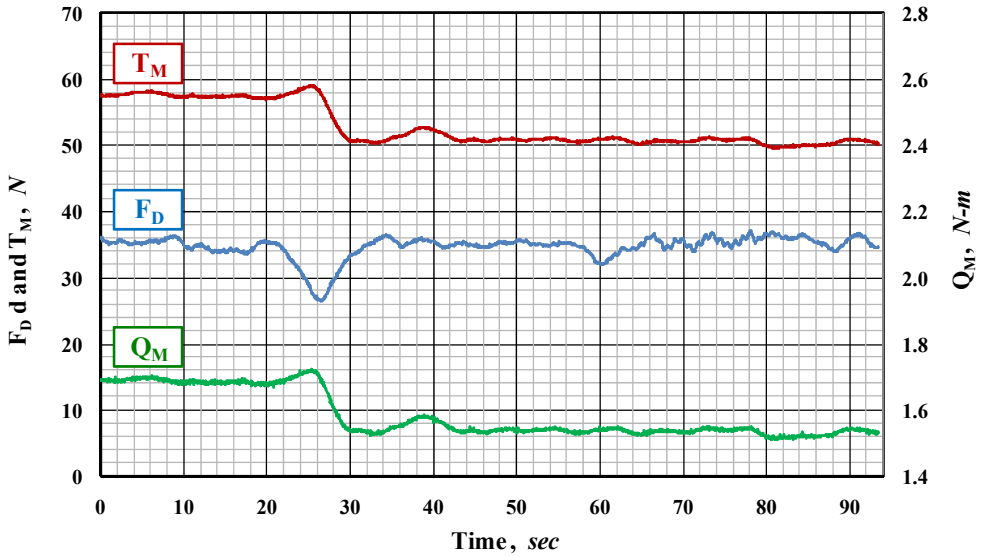

Fig. 21 Chang in the physical quantities measured during self-propulsion tests at V_S = 14.5*knots* and mean t_{AL} = 8.2*mm* in the air injection condition II.

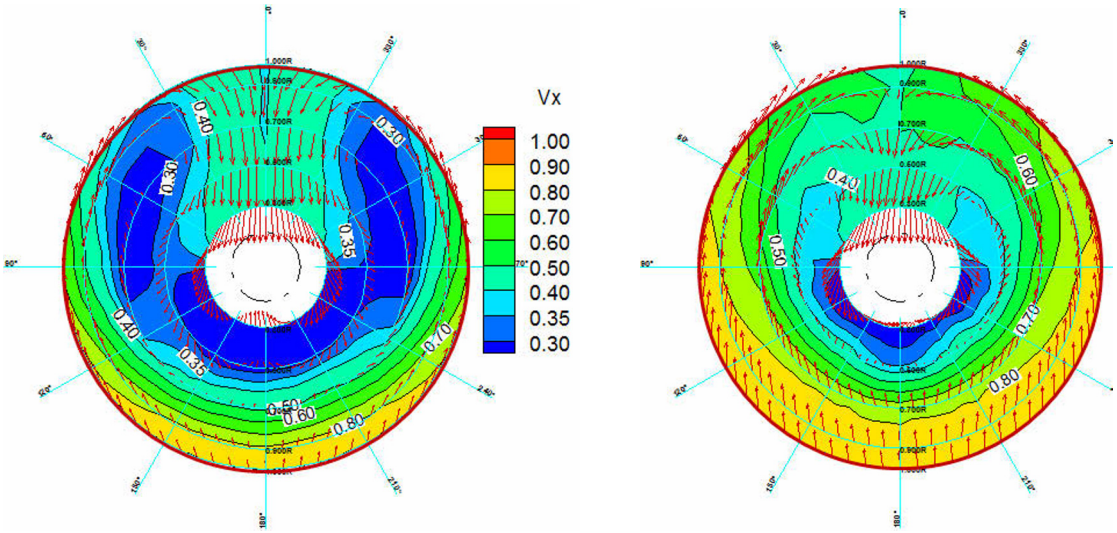

w_N = 0.573 w_N = 0.413

(a) Without air injection. (b) With air injection.

Fig. 22 Nominal wake distributions at V_S = 14.5*knots* (mean t_{AL} = 8.2*mm* in the air injection condition II).

Nominal wake distributions were measured with the underwater PIV system of SSMB to investigate the reason why the propeller thrust and torque were reduced. As shown in Fig. 22, the level of the axial velocity increased significantly and the nominal wake fraction, w_N was changed into 0.413 from 0.573 when an air layer was generated on the bottom of the hull. In addition, downward flow in the upper area of the propeller shaft decreased. It is thought that increase in the momentum of the flow along the hull bottom by the frictional resistance reduction made the flow into the propeller plane accelerated and this led to the reduction in the propeller thrust and torque.

Differences of main self-propulsion factors were compared in Fig. 23. There were not any significant changes, less than 1%, in the relative rotative efficiency (η_R) and thrust deduction fraction (t), while the full scale wake fraction (w_{TS}) decreased considerably due to flow acceleration effect by air layers generated on the bottom of the hull as mentioned in the nominal wake distributions. The hull efficiency (η_H) decreased by about 5~6%, but open water efficiency increased by about 5% as the

propeller loading was reduced. Consequently, the quasi-propulsive efficiency (η_D) was reduced by about 0.6~0.9% compared with the case that air was not injected. This coincides with a preceding study that the loss in the propulsive efficiency was assumed to be about 1% when a small amount of bubbles flows into the top of the propeller plane (Kawakita et al., 2011). Finally, the reduction in the delivered power was estimated to be about 7~9.5% in the speeds range of 13.0~16.0*knots* as shown in Fig. 24.

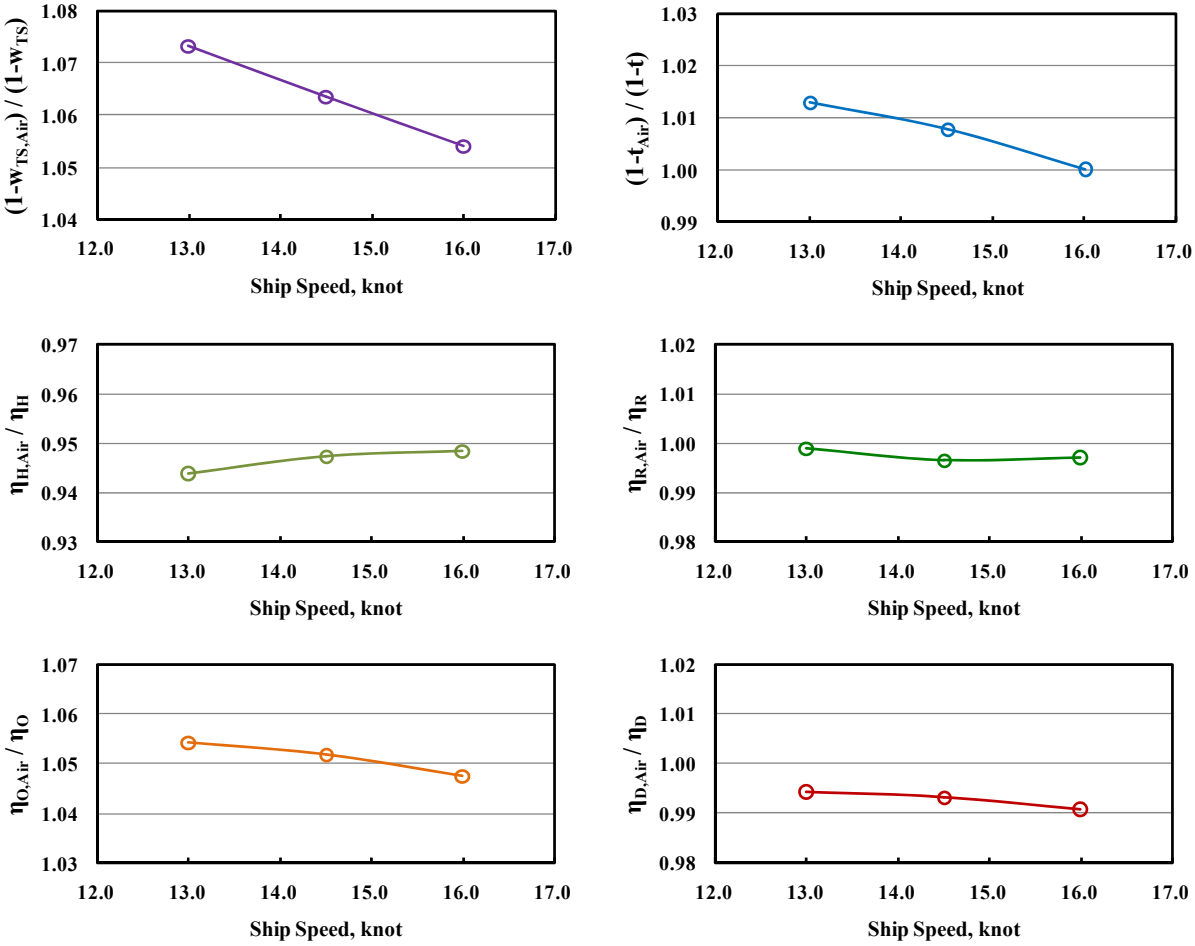

Fig. 23 Changes in self-propulsion factors at mean t_{AL} = 8.2*mm* in the air injection condition II.

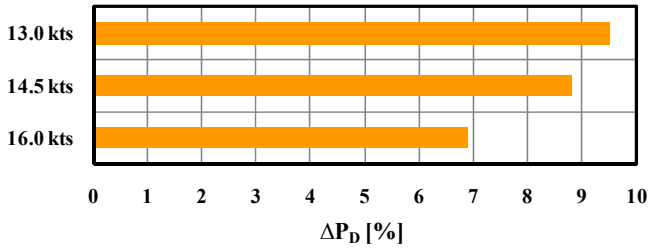

Fig. 24 Reduction in the delivered power at mean t_{AL} = 8.2*mm* in the air injection condition II.

Net power savings

The required power for air injection, P_{Air} was estimated as the power needed to compress a given quantity of air at standard condition, 1*atm* and 25°*C* via a polytropic process according to Eq. (18) (Pinches and Callear, 1997; Ceccio and Makihärju, 2012).

$$P_{Air} = \frac{Q_{Std.Air}}{\eta_C} \cdot p_1 \cdot \left(\frac{n}{n-1} \right) \cdot \left\{ \left(\frac{p_2}{p_1} \right)^{\frac{n-1}{n}} - 1 \right\} \tag{18}$$

In the above equation, $Q_{Std.Air}$ is the full scale flow rate of air at standard condition and η_C is an efficiency of an air compressor, n is the polytropic index assumed to be 1.4 corresponding to the isentropic process. p_1 is the atmospheric pressure and p_2 is the delivery pressure to which air needs to be compressed for air injection on the bottom of the hull.

Using the hydrostatic pressure acting on the water depth corresponding to the bottom of the model ship and the water temperature, the mass flow rates of air measured by the flow meters were converted into the volume flow rates of air in model scale, and the values of the ideal air layer thickness in model scale were obtained. Then, the full scale volume flow rates were estimated on the assumption that the ideal air layer thickness, t_{AL} in Eq. (19) should be roughly the same in the model and full scale. Finally, the full scale flow rates of air at standard condition, $Q_{Std.Air}$ in Eq. (18) were obtained from the full scale volume flow rate, Q_{Air} under a polytropic process with n = 1.4.

$$t_{AL} = \frac{Q_{Air}}{V_S \cdot B_{Unit}} \tag{19}$$

In the above equation, Q_{Air}, V_S, and B_{Unit} are volume flow rate of injected air, ship speed, and the width of the air injection unit respectively.

The efficiency of an air compressor, η_C in Eq. (18) was assumed to be 0.75 from the comparison with the driving motor power values of air compressors on the market. The delivery pressure of air, p_2 was obtained as the sum of the atmospheric pressure, the hydrostatic pressure at the hull bottom where air is injected, and the pressure drop due to piping losses, Δp according to Eq. (20).

$$p_2 = p_1 + \rho_S \cdot g \cdot T + \Delta p \tag{20}$$

In Eq. (20), ρ_S is the density of sea water at water temperature 15°*C* and g is the acceleration of gravity. T is the draft of the ship, here 11.2*m*. In this study, the pressure drop, Δp due to piping losses was assumed to be 1 *bar* equivalent to the hydrostatic pressure at 10*m* water depth.

$$\Delta P_{Net} = \Delta P_D - \left(\frac{P_{Air}}{P_D} \times 100 \right) \tag{21}$$

Finally, the expected net power savings, ΔP_{Net} were estimated to be 5~6% in the speed range of 13.0~16.0*knots* according to Eq. (21) as shown in Fig. 25.

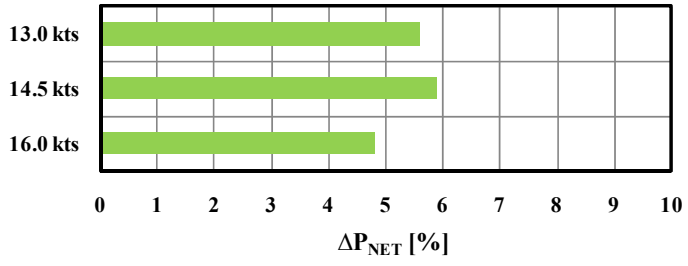

Fig. 25 Net power savings at mean t_{AL} = 8.2*mm* in the air injection condition II.

CONCLUSIONS

The experiments to generate air layers on the lower surface of a flat plate in the large water tunnel were conducted. From the experiments, it was ascertained that a transitional air layer generated by air injection on the bottom of the hull, where patches of continuous air layer coexist with air bubbles, can be utilized as one of effective means to reduce the frictional resistance of ships. It is necessary to make injected air spread evenly after injection to increase persistence length of the frictional resistance reduction.

For a wide beam 66K DWT Supramax bulk carrier, net power savings were estimated from the resistance and self-propulsion tests in the towing tank, considering power consumption for air injection. The resistance and propulsion performance was estimated on the assumption that air layers does not change the residuary resistance. In addition, it was assumed that the reduction ratio of the frictional resistance and the ideal air layer thickness in the full scale are maintained with the same level as the model scale. Full scale correction of wake fraction was done according to a procedure based on Tanaka-Sasajima's method. The power consumption for air injection was estimated as the required power to compress a given quantity of air at standard condition, 1*atm* and 25°*C* via a polytropic process.

From the tests, it was estimated that the effective power was reduced by about 8~10% and the delivered power was reduced by 7~9.5% approximately due to the loss in the quasi-propulsive efficiency, less than 1%. Finally, net power savings were estimated to be around 5~6%, considering the required power for air injection, 2~4% of the shaft power when air was not injected.

It is thought that air lubrication with air layers generated on the bottom of ships has great potential for power savings if there is not any significant performance deterioration in real sea conditions. Accordingly, the performance in waves will be investigated to assess more rigorously the feasibility of the air lubrication technique as an effective energy saving means for ships.

ACKNOWLEDGEMENTS

This research was carried out in the research grant, “Development of the key technology for a ship drag reduction and propulsion efficiency improvement (No.10040030)”, partially funded by the Ministry of Trade, Industry and Energy.

REFERENCES

Allenström, B. and Leer-Andersen, M., 2010. Model tests with air lubrication. *International Conference on Ship Drag Reduction SMOOTH-SHIPS*, Istanbul, Turkey, 20-21 May 2010, Paper No.1.

Bushnell, D.M. and Hefner, J.N., 1990. *Viscous drag reduction in boundary layers, progress in astronautics and aeronautics, 123*. Washington, D.C.: The American Institute of Aeronautics and Astronautics, Inc.

Ceccio, S.L., 2010a. Frictional drag reduction of external flows with bubble and gas injection. *Annual Review of Fluid Mechanics*, 42, pp.183-203.

Ceccio, S.L., Perlin, M. and Elbing, B.R., 2010b. A cost-benefit analysis for air layer drag reduction. *International Conference on Ship Drag Reduction SMOOTH-SHIPS*, Istanbul, Turkey, 20-21 May 2010, Paper No.4.

Ceccio, S.L. and Makihärju, S.A., 2012. *Air lubrication drag reduction on great lakes ships, Report of Great Lakes Maritime Research Institute*. Michigan: Department of Naval Architecture and Marine Engineering, University of Michigan.

Elbing, B.R., Winkel, E.S., Lay, K., Ceccio, S.L., Dowling, D.R. and Perlin, M., 2008. Bubble-induced skin friction drag reduction and the abrupt transition to air-layer drag reduction. *Journal of Fluid Mechanics*, 612, pp.201-236.

Foeth, E.J., 2008. Decreasing frictional resistance by air lubrication. *20th International HISWA Symposium on Yacht Design and Yacht Construction*, Amsterdam, Netherlands, 17-18 November 2008.

Foeth, E.J., Eggers, R. and Ouadvlieg, F.H.H.A., 2010. The efficacy of air-bubble lubrication for decreasing friction resistance. *International Conference on Ship Reduction SMOOTH-SHIPS*, Istanbul, Turkey, 20-21 May 2010, Paper No.12.

Hoang, C.L., Toda, Y. and Sanada, Y., 2009. Full scale experiment for frictional resistance reduction using air lubrication method. *19th International Offshore and Polar Engineering (ISOPE) Conference*, Osaka, Japan, pp.812-817.

Insel, M., Gokcay, S., and Helvacioglu, I.H., 2010. Flow analysis of an air injection through discrete air lubrication. *International Conference on Ship Drag Reduction SMOOTH-SHIPS*, Istanbul, Turkey, 20-21 May 2010, Paper No.13.

Kawakita, C., Takano, S., Kodan, Y. and Mizokami, S., 2011. Experimental investigation of the behavior of injected air on the ship bottom and its influence on propeller. *Journal of Japan Society of Naval Architects and Ocean Engineers*, 12, pp.43-50.

Latorre, R., 1997. Ship hull drag reduction using bottom air injection. *Ocean Engineering*, 24(2), pp.161-175.

Mizokami, S., Kawakita, C., Kodan, Y., Takano, S., Higasa, S. and Shigenaga, R., 2010. Experimental study of air lubrication method and verification of effects on actual hull by means of sea trial. *Mitsubishi Heavy Industries Technical Review*, 47(3), pp.41-47.

Mizokami, S., Kawakita, C., Kodan, Y., Takano, S., Higasa, S. and Shigenaga, R., 2011. Development of air lubrication system and verification by the full scale ship test. *Journal of Japan Society of Naval Architects and Ocean Engineers*, 12, pp.69-77.

Pinches, M.J. and Callear, B.J., 1997. *Power pneumatics*. New Jersey: Prentice Hall.

Tanaka, T., 2011. Green technologies featuring the Mitsubishi air lubrication system. *1st World NAOE Forum*, Osaka, Japan, 20-21 May 2010, pp.43-59.

Thill, C., 2010. A long road mapping drag reduction. *International Conference on Ship Drag Reduction SMOOTH-SHIPS*, Istanbul, Turkey, 20-21 May 2010.